

# 4.0-Å resolution cryo-EM structure of the mammalian chaperonin TRiC/CCT reveals its unique subunit arrangement

Yao Cong<sup>a</sup>, Matthew L. Baker<sup>a</sup>, Joanita Jakana<sup>a</sup>, David Woolford<sup>a</sup>, Erik J. Miller<sup>b</sup>, Stefanie Reissmann<sup>b,2</sup>, Ramya N. Kumar<sup>b</sup>, Alyssa M. Redding-Johanson<sup>c</sup>, Tanveer S. Batth<sup>c</sup>, Aindrila Mukhopadhyay<sup>c</sup>, Steven J. Ludtke<sup>a</sup>, Judith Frydman<sup>b</sup>, and Wah Chiu<sup>a,1</sup>

<sup>a</sup>National Center for Macromolecular Imaging, Verna and Marrs McLean Department of Biochemistry and Molecular Biology, Baylor College of Medicine, Houston, TX 77030; <sup>b</sup>Department of Biology and BioX Program, Stanford University, Stanford, CA 94305; and <sup>c</sup>Physical Biosciences Division, Lawrence Berkeley National Laboratory, Berkeley, CA 94720

Communicated by Michael Levitt, Stanford University School of Medicine, Stanford, CA, December 7, 2009 (received for review October 21, 2009)

The essential double-ring eukaryotic chaperonin TRiC/CCT (TCP1-ring complex or chaperonin containing TCP1) assists the folding of ~5–10% of the cellular proteome. Many TRiC substrates cannot be folded by other chaperonins from prokaryotes or archaea. These unique folding properties are likely linked to TRiC's unique heterooligomeric subunit organization, whereby each ring consists of eight different paralogous subunits in an arrangement that remains uncertain. Using single particle cryo-EM without imposing symmetry, we determined the mammalian TRiC structure at 4.7-Å resolution. This revealed the existence of a 2-fold axis between its two rings resulting in two homotypic subunit interactions across the rings. A subsequent 2-fold symmetrized map yielded a 4.0-Å resolution structure that evinces the densities of a large fraction of side chains, loops, and insertions. These features permitted unambiguous identification of all eight individual subunits, despite their sequence similarity. Independent biochemical near-neighbor analysis supports our cryo-EM derived TRiC subunit arrangement. We obtained a C $\alpha$  backbone model for each subunit from an initial homology model refined against the cryo-EM density. A subsequently optimized atomic model for a subunit showed ~95% of the main chain dihedral angles in the allowable regions of the Ramachandran plot. The determination of the TRiC subunit arrangement opens the way to understand its unique function and mechanism. In particular, an unevenly distributed positively charged wall lining the closed folding chamber of TRiC differs strikingly from that of prokaryotic and archaeal chaperonins. These interior surface chemical properties likely play an important role in TRiC's cellular substrate specificity.

asymmetric reconstruction | atomic model | subunit structure

Defective protein folding is emerging as the molecular basis underlying a growing number of human diseases, ranging from cancer and heart disease (1) to aggregation-linked neurodegenerative diseases such as Alzheimer's, Huntington, and mad cow disease (2, 3). The eukaryotic group II chaperonin TRiC (also known as CCT) is a central mediator of cytosolic protein folding and assembly (4, 5). TRiC also appears important for the prevention of protein aggregation and toxicity (6–8). TRiC is essential for cell viability, as it assists the folding of many essential proteins, including actin, tubulin, and many cell cycle regulators and signaling molecules (9, 10). Notably, a number of TRiC substrates cannot be folded by other chaperonins, suggesting that TRiC possesses unique structural and mechanistic properties that distinguish it functionally from other chaperonins (11, 12).

All chaperonins share a double-ring architecture, where each ring contains a central cavity that binds and folds substrate proteins. TRiC, a 1 MDa group II chaperonin, facilitates folding through the ATPase driven closure of a built-in lid that encloses the substrate in the central chamber (13–16). Each ring of TRiC

consists of eight distinct but related subunits sharing 27–39% sequence identity (Fig. S1) (13, 17). In contrast, bacterial (18) and archaeal chaperonins (19) only have 1–3 different types of subunits, and for those archaea with three types of subunits, it is unclear whether in the natural organism they form homo- or heterooligomeric chaperonins (20). The divergence of TRiC subunits occurred early in the evolution of eukaryotes, because all eukaryotes sequenced to date carry genes for all eight subunits; orthologs of the various subunits across species are more similar than paralogs within a single species (17). Having eight distinct subunits may have allowed the diversification of substrate binding sites and activities within the ring of TRiC. Actin, tubulin (21, 22), Huntingtin (8), and the von Hippel–Lindau tumor suppressor (23) are all recognized by distinct subsets of TRiC subunits through specific motifs; this directed binding may provide specificity for TRiC in the folding process. Accordingly, elucidating the subunit arrangement within the complex is essential to determine how TRiC affects the conformation and folding pathway of its substrates.

Understanding the molecular basis of the specific folding capacity of TRiC has been hindered by the paucity of structural information on this complex. An intraring subunit arrangement proposed from analysis of spontaneously dissociated TRiC complexes remains untested (24). Previous cryo-EM studies of TRiC achieved only up to ~15-Å resolution with imposed 8-fold symmetry (13, 25, 26), inadequate to resolve the asymmetry between the eight structurally similar subunits. Here we present a high-resolution cryo-EM structure of mammalian TRiC, derived without imposing any symmetry among the eight subunits. Our analysis reveals (*i*) a 2-fold axis of symmetry between the two rings of TRiC, and (*ii*) its intraring subunit arrangement. The structure-derived subunit arrangement of TRiC is supported by cross-linking analysis. Our study provides a structural baseline to elucidate the complicated mechanisms of substrate recognition, folding and cooperativity in TRiC.

Author contributions: Y.C., J.F., and W.C. designed research; Y.C., M.L.B., J.J., E.J.M., S.R., R.N.K., A.M.R.-J., T.S.B., and A.M. performed research; Y.C., D.W., and S.J.L. contributed new reagents/analytic tools; Y.C., M.L.B., E.J.M., A.M., S.J.L., J.F., and W.C. analyzed data; Y.C., M.L.B., E.J.M., A.M., S.J.L., J.F., and W.C. wrote the paper.

Conflict of interest statement: The Sponsor is an investigator of the Nanomedicine Development Center with the support of National Institutes of Health Grant (5PN2EY016525), which is directed by the corresponding author.

Data deposition: The density maps and models have been deposited in the Electron Microscopy Data Bank (accession numbers EMD-5145 and EMD-5148) and Protein Data Bank, [www.pdb.org](http://www.pdb.org) (PDB ID codes 3KTT and 3IYG).

<sup>1</sup>To whom correspondence should be addressed. E-mail: wah@bcm.edu.

<sup>2</sup>Present address: Max Planck Institute for Terrestrial Microbiology, Marburg, Germany D-35043.

This article contains supporting information online at [www.pnas.org/cgi/content/full/0913774107/DCSupplemental](http://www.pnas.org/cgi/content/full/0913774107/DCSupplemental).





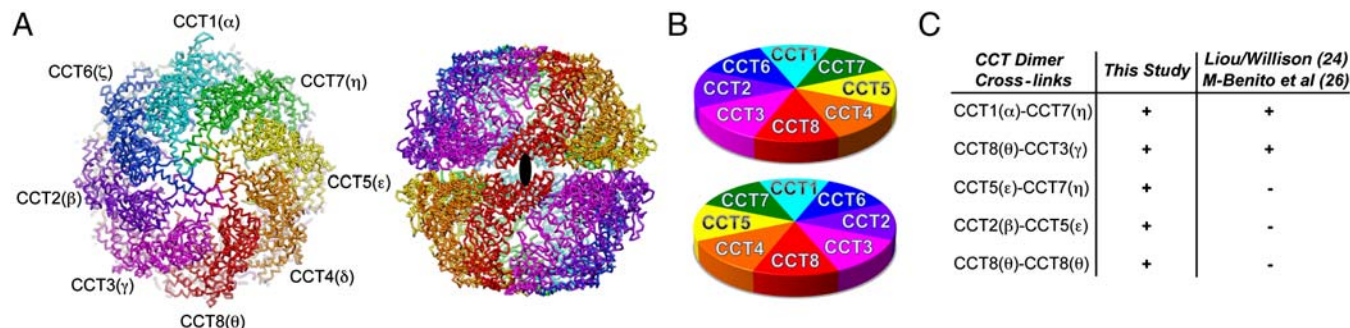


**Fig. 3.** The optimized  $C\alpha$  model of the entire TRiC complex with its 16 subunits in the spatial arrangement determined by our cryo-EM structure. (A) End-on and side views of the TRiC complex. Same color scheme as in Fig. 1. (B) Cartoon diagram illustrating the arrangement of the 16 subunits in the two rings. We denote the TRiC subunits only by their CCT number. (C) Summary of near neighbors TRiC subunits identified by chemical cross-linking. Neighboring subunit pairs consistent with the indicated models are marked with a “+,” and those inconsistent with the indicated models are marked with a “-.”

arrangement was provided by chemical cross-linking of adjacent subunits in the intact chaperonin (Fig. S5, Table S1, and *SI Methods*). Formaldehyde, which has one of the shortest cross-linking spans ( $<3 \text{ \AA}$ ) was used to yield specific covalent adducts between neighboring chaperonin subunits both within a single ring and across the rings (30, 31). Given the similarity in molecular weight and isoelectric point of the TRiC subunits, and hence of their covalently linked dimers, we separated the cross-linked subunits by 2D-PAGE (Fig. S5B). Well-separated spots corresponding in size to a dimer of TRiC subunit were excised, and MS was used to identify the subunits present in each spot. Covalently linked near neighbors were inferred from these spots that had multiple peptides corresponding to only two TRiC subunits. This approach identified several unambiguous neighboring subunit pairs (Fig. 3C, Fig. S5C, and Table S1), all of which were consistent with our cryo-EM-derived subunit arrangement (Fig. 3B). Of note, several of these determined cross-links were inconsistent with previously proposed subunit arrangement of TRiC (24, 26). For instance, the prominent CCT2(β)-CCT5(ε) cross-link (Fig. 3C and Fig. S5C) is fully inconsistent with previous models (24, 26), but agrees with an interring contact proposed by our cryo-EM-derived structure (Fig. 3B). In case of the CCT8(θ)-CCT8(θ) dimer, obtained by cross-linking (Fig. 3C and Fig. S5C), this covalent adduct can only arise from the homotypic interring contact of two CCT8(θ) subunits, as shown by our cryo-EM-derived structure (Fig. 3B). This biochemical analysis thus supports our cryo-EM-derived subunit arrangement and model.

**Optimization and Validation of the TRiC Model.** Our cryo-EM structure clearly resolves many side chains within the subunits. In X-ray crystallography, density maps determined at  $\sim 4.0\text{-\AA}$  resolution range are often considered marginal for determining the atomistic structures (32). However, recent studies have shown that it is indeed possible to reliably build a de novo  $C\alpha$  model directly from cryo-EM density map in this resolution range (28, 33). It should also be noted that our density map (Fig. 1B) was directly computed from the raw images (Fig. 1A) and not biased by any atomic model.

In order to assess the ultimate quality of our map and model, we optimized the full atomic model from the initial  $C\alpha$  chain trace by matching it to the map and the visible side-chain densities for three randomly chosen subunits: CCT2(β), CCT1(α), and CCT7(η). Fig. 4A shows the atomic model of the CCT2(β) subunit. The Ramachandran plot of this optimized model shows that over 95% of the main chain dihedral angles fall within allowable regions (Fig. 4B), demonstrating the quality of the final model to follow the protein stereochemistry. Optimized atomic models of the other two subunits show similar quality.

To further validate our model, we compare the only available TRiC domain crystal structure [i.e., the apical domain of mouse CCT3(γ) (34)] with our corresponding model. Because the crystal

structure was not used as a template to build our model, 1GML can serve as a quality check. The good match between our model and 1GML (Fig. S6) validates the reliability of our model and thus, the quality of our map.

## Discussion

Unlike most chaperonins, which have one to three distinct subunits, TCP1-ring complex or chaperonin containing TCP1 (TRiC/CCT) has eight distinct, but similar, subunits. The subunits are sufficiently similar that determining individual particle orientation with sufficient precision would require very high resolution. Considering also the roughly spherical shape of the both-ring-closed conformation (Fig. 1A and B), the determination of particle orientation of TRiC presented even more challenges than other asymmetric structures studied so far by cryo-EM. Approximately 35% of the  $\sim 160,000$  particles lacked sufficient contrast even at this resolution to unambiguously assign their orientation. Identifying and eliminating these particles using custom software

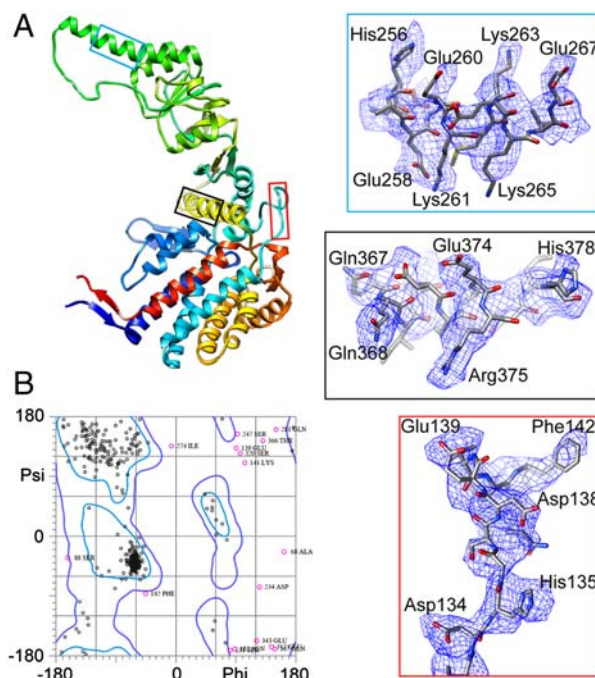


**Fig. 4.** The atomic model of CCT2(β) subunit and the match between the  $a_{iii}$  density and the model. (A) Optimized atomic model of CCT2(β) with the N terminus in blue and C terminus in red. Zoom in views show the match between three stretches of densities highlighted in different color frames and the corresponding model. (B) The Ramachandran plot of the CCT2(β) model calculated by MolProbity (48) shows that over 95% of the dihedral angles fall within allowable regions.



## Materials and Methods

TRiC sample purification (42) and cryoEM sample preparation follow our established procedures (14). Data were collected on a JEM3200FSC electron microscope with an in-column energy filter (energy slit of 15 eV) under the following conditions: 300 kV, ~50,000x magnification, ~20 electrons/Å<sup>2</sup> dose, and 101 K specimen temperature. Images were recorded on Kodak SO163 film and digitized on a Nikon 9000 ED scanner with a 1.2 Å/pixel sampling. The majority of the defocus ranges from 1.2–2.7 μm.

Approximately 160,000 particles were selected from 1,500 micrographs with the EMAN2 tool *e2boxer*. Contrast transfer function parameters were determined using *ctfit* of EMAN (27, 28, 43). A recently developed FRM2D algorithm for image alignment (36, 37, 44), available in EMAN 1.8+ (*frm2d* option in *refine* program), was adopted in the refinement steps. We used a previously determined 15-Å resolution 8-fold symmetrized map of closed TRiC (13) as the initial model of the reconstruction. Other than that, in

the asymmetric reconstruction and refinement process, no symmetry was imposed. The final map was computed from ~101,000 particle images, after eliminating particles that were not consistently classified in the same orientation between iterations. The map resolution was based on the 0.5 Fourier shell correlation (FSC) criterion (45). The final map was filtered and scaled to optimized map resolvability (46, 47).

Detailed procedures about map similarity analysis, homology model building and model optimization, and cross-linking and nearest-neighbor analysis are provided in *SI Materials and Methods*.

**ACKNOWLEDGMENTS.** We would like to thank Dr. Michael F. Schmid for very helpful discussions and suggestions. This research is supported by grants from National Institutes of Health (PN1EY016525, P41RR02250, and GMR01-074074) and National Science Foundation (IIS-0705644), and Department of Energy Contract DE-AC02-05CH11231.

1. Scott MD, Frydman J (2003) Aberrant protein folding as the molecular basis of cancer. *Method Mol Biol* 232:67–76.
2. Morimoto RI (2008) Proteotoxic stress and inducible chaperone networks in neurodegenerative disease and aging. *Genes Dev* 22:1427–1438.
3. Dobson CM (2004) Principles of protein folding, misfolding and aggregation. *Semin Cell Dev Biol* 15:3–16.
4. Frydman J (2001) Folding of newly translated proteins in vivo: The role of molecular chaperones. *Annu Rev Biochem* 70:603–647.
5. Hartl FU, Hayer-Hartl M (2009) Converging concepts of protein folding in vitro and in vivo. *Nat Struct Mol Biol* 16:574–581.
6. Behrends C, et al. (2006) Chaperonin TRiC promotes the assembly of polyQ expansion proteins into nontoxic oligomers. *Mol Cell* 23:887–897.
7. Kitamura A, et al. (2006) Cytosolic chaperonin prevents polyglutamine toxicity with altering the aggregation state. *Nat Cell Biol* 8:1163–1170.
8. Tam S, Geller R, Spiess C, Frydman J (2006) The chaperonin TRiC controls polyglutamine aggregation and toxicity through subunit-specific interactions. *Nat Cell Biol* 8:1155–1162.
9. Dunn AY, Melville MW, Frydman J (2001) Review: Cellular substrates of the eukaryotic chaperonin TRiC/CCT. *J Struct Biol* 135:176–184.
10. Yam AY, et al. (2008) Defining the TRiC/CCT interactome links chaperonin function to stabilization of newly made proteins with complex topologies. *Nat Struct Mol Biol* 15:1255–1262.
11. Leroux MR, Hartl FU (2000) Protein folding: Versatility of the cytosolic chaperonin TRiC/CCT. *Curr Biol* 10:R260–264.
12. Spiess C, Meyer AS, Reissmann S, Frydman J (2004) Mechanism of the eukaryotic chaperonin: protein folding in the chamber of secrets. *Trends Cell Biol* 14:598–604.
13. Booth CR, et al. (2008) Mechanism of lid closure in the eukaryotic chaperonin TRiC/CCT. *Nat Struct Mol Biol* 15:746–753.
14. Meyer AS, et al. (2003) Closing the folding chamber of the eukaryotic chaperonin requires the transition state of ATP hydrolysis. *Cell* 113:369–381.
15. Reissmann S, Parnot C, Booth CR, Chiu W, Frydman J (2007) Essential function of the built-in lid in the allosteric regulation of eukaryotic and archaeal chaperonins. *Nat Struct Mol Biol* 14:432–440.
16. Gutsche I, Essen LO, Baumeister W (1999) Group II chaperonins: New TRiC(k)s and turns of a protein folding machine. *J Mol Biol* 293:295–312.
17. Archibald JM, Blouin C, Doolittle WF (2001) Gene duplication and the evolution of group II chaperonins: Implications for structure and function. *J Struct Biol* 135:157–169.
18. Xu Z, Horwich AL, Sigler PB (1997) The crystal structure of the asymmetric GroEL-GroES-(ADP)<sub>7</sub> chaperonin complex. *Nature* 388:741–750.
19. Ditzel L, et al. (1998) Crystal structure of the thermosome, the archaeal chaperonin and homolog of CCT. *Cell* 93:125–138.
20. Kapatai G, et al. (2006) All three chaperonin genes in the archaeon *Haloferax volcanii* are individually dispensable. *Mol Microbiol* 61:1583–1597.
21. Valpuesta JM, Martin-Benito J, Gomez-Puertas P, Carrascosa JL, Willison KR (2002) Structure and function of a protein folding machine: The eukaryotic cytosolic chaperonin CCT. *FEBS Lett* 529:11–16.
22. Etchells SA, et al. (2005) The cotranslational contacts between ribosome-bound nascent polypeptides and the subunits of the hetero-oligomeric chaperonin TRiC probed by photocross-linking. *J Biol Chem* 280:28118–28126.
23. Spiess C, Miller EJ, McClellan AJ, Frydman J (2006) Identification of the TRiC/CCT substrate binding sites uncovers the function of subunit diversity in eukaryotic chaperonins. *Mol Cell* 24:25–37.
24. Liou AK, Willison KR (1997) Elucidation of the subunit orientation in CCT (chaperonin containing TCP1) from the subunit composition of CCT micro-complexes. *EMBO J* 16:4311–4316.
25. Llorca O, et al. (2001) The “sequential allosteric ring” mechanism in the eukaryotic chaperonin-assisted folding of actin and tubulin. *EMBO J* 20:4065–4075.
26. Martin-Benito J, et al. (2007) The inter-ring arrangement of the cytosolic chaperonin CCT. *EMBO Rep* 8:252–257.
27. Ludtke SJ, Baldwin PR, Chiu W (1999) EMAN: Semiautomated software for high-resolution single-particle reconstructions. *J Struct Biol* 128:82–97.
28. Ludtke SJ, et al. (2008) De novo backbone trace of GroEL from single particle electron cryomicroscopy. *Structure* 16:441–448.
29. Iizuka R, et al. (2004) Role of the helical protrusion in the conformational change and molecular chaperone activity of the archaeal group II chaperonin. *J Biol Chem* 279:18834–18839.
30. Nadeau OW, Carlson GM (2005) Protein interactions captured by chemical cross-linking. *Protein-Protein Interactions: A Molecular Cloning Manual*, ed Golemis EA (Cold Spring Harbor Laboratory Press, Cold Spring Harbor, New York), 2nd Ed, pp 105–128.
31. Rice NA, Nadeau OW, Yang Q, Carlson GM (2002) The calmodulin-binding domain of the catalytic  $\gamma$  subunit of phosphorylase kinase interacts with its inhibitory alpha subunit: Evidence for a Ca<sup>2+</sup> sensitive network of quaternary interactions. *J Biol Chem* 277:14681–14687.
32. Blow D (2002) *Outline of Crystallography for Biologists* (Oxford University Press, New York), pp 191–204.
33. DiMaio F, Tyka MD, Baker ML, Chiu W, Baker D (2009) Refinement of protein structures into low-resolution density maps using rosetta. *J Mol Biol* 392:181–190.
34. Pappenberger G, et al. (2002) Crystal structure of the CCTgamma apical domain: Implications for substrate binding to the eukaryotic cytosolic chaperonin. *J Mol Biol* 318:1367–1379.
35. Tang G, et al. (2007) EMAN2: An extensible image processing suite for electron microscopy. *J Struct Biol* 157:38–46.
36. Cong Y, Kovacs JA, Wriggers W (2003) 2D fast rotational matching for image processing of biophysical data. *J Struct Biol* 144:51–60.
37. Cong Y, et al. (2005) Fast rotational matching of single-particle images. *J Struct Biol* 152:104–112.
38. Miller EJ, Meyer AS, Frydman J (2006) Modeling of possible subunit arrangements in the eukaryotic chaperonin TRiC. *Protein Sci* 15:1522–1526.
39. Rivenzon-Segal D, Wolf SG, Shimon L, Willison KR, Horovitz A (2005) Sequential ATP-induced allosteric transitions of the cytoplasmic chaperonin containing TCP-1 revealed by EM analysis. *Nat Struct Mol Biol* 12:233–237.
40. Tang YC, et al. (2006) Structural features of the GroEL-GroES nano-cage required for rapid folding of encapsulated protein. *Cell* 125:903–914.
41. Horwich AL, Fenton WA, Chapman E, Farr GW (2007) Two families of chaperonin: Physiology and mechanism. *Annu Rev Cell Dev Biol* 23:115–145.
42. Ferreyra RG, Frydman J (2000) Purification of the cytosolic chaperonin TRiC from bovine testis. *Method Mol Biol* 140:153–160.
43. Ludtke SJ, Jakana J, Song JL, Chuang DT, Chiu W (2001) A 11.5 Å single particle reconstruction of GroEL using EMAN. *J Mol Biol* 314:253–262.
44. Cong Y, et al. (2009) Structural mechanism of SDS-induced enzyme activity of scorpion hemocyanin revealed by electron cryomicroscopy. *Structure* 17:749–758.
45. Harauz G, van Heel M (1986) Exact filters for general geometry three dimensional reconstruction. *Optik* 73:146–156.
46. Rosenthal PB, Henderson R (2003) Optimal determination of particle orientation, absolute hand, and contrast loss in single-particle electron cryomicroscopy. *J Mol Biol* 333:721–745.
47. Fernandez JJ, Luque D, Caston JR, Carrascosa JL (2008) Sharpening high resolution information in single particle electron cryomicroscopy. *J Struct Biol* 164:170–175.
48. Davis IW, et al. (2007) MolProbity: All-atom contacts and structure validation for proteins and nucleic acids. *Nucleic Acids Res* 35:W375–383.